Kinetic modeling of enzymatic fluorescence retrieval of a fluorogenic probe for Penicillin-G-Acylase

Roshanasan, Ardeshir; Yu, Wang; Katsas, Nektarios; van Esch, Jan H.

DOI
10.1016/j.bej.2025.109780

Publication date
2025

Document Version
Final published version

Published in
Biochemical Engineering Journal

Biochemical Engineering Journal 222 (2025) 109780

Contents lists available at ScienceDirect

Biochemical Engineering Journal

journal homepage: www.elsevier.com/locate/bej

Short Communication

Kinetic modeling of enzymatic fluorescence retrieval of a fluorogenic probe for Penicillin-G-Acylase

Ardeshir Roshanasan [a], Wang Yu [b], Nektarios Katsas [c], Jan H. van Esch [a,*]

[a] Department of Chemical Engineering, Delft University of Technology, Van der Maasweg 9, 2629 HZ Delft, The Netherlands
[b] Department of Detection and Diagnosis Technology Research, Guangzhou National Laboratory, Guangzhou, Guandong, 510000, PR China
[c] Department of Chemical Engineering, University of Patras, Caratheodory 1, GR 265 04 Patras, Greece

ARTICLE INFO

Keywords:
Enzyme kinetics
Fluorogenic probes
Penicillin-G-Acylase (PGA)
Inhibitory kinetics
Uni-bi reaction mechanism

ABSTRACT

This work presents the development and validation of a kinetic model describing the enzymatic hydrolysis of a specifically designed fluorogenic probe for free Penicillin-G Acylase (PGA). The model construction involved tracking reaction kinetics through UV–Vis spectroscopy, identifying product-induced inhibitory effects, and employing initial velocity analysis alongside parameter estimation techniques. The kinetic model was structured around a simple ordered uni-bi mechanism comprising three reversible reaction steps. Validation of the model was performed through spectrofluorometric measurements, successfully predicting the fluorescence intensity progression resulting from the enzymatic cleavage of the probe.

1. Introduction

Retrieving fluorescent signals could be effectively utilized for detection and sensory purposes. This is achieved by implementation of fluorogenic probes which are principally designer quenched fluorophore molecules. They are designed in a way where the quenching would only wear off via the specific reaction of the fluorogenic probe with the target [1], consequently reinstating the fluorescence. The quencher is either a reactive group which loses its quenching capability once it forms a bond with the target [2], or it is a non-reactive entity which leaves the probe, once the probe reacts with the target [3]. Measuring the retrieved fluorescence intensity over time unveils information about the target and its reaction with the fluorogenic probe. Such targets are generally proteins and in particular enzymes. Consequently, this type of probes have found applications in cellular imaging [4,5], and in studying the cellular events and enzyme detection [6–8]. For instance, Luo et al. (2024) [9] introduced a two-photon fluorescent probe for highly selective and rapid detection, facilitating real-time imaging of inflammatory responses and tumor conditions. Recently, Su et al. (2025) [10] reported on a β-galactosidase-activated near-infrared fluorescent probe, capable of accurately monitoring cellular senescence both in vitro and in vivo, thus highlighting the growing potential of fluorogenic probes for the precise diagnosis and monitoring of diseases. Other design strategies by Zhao et al. (2023) [11] and Liu et al. (2024) [12] crossed the boundaries of detection, leading to designing probes which demonstrate photodynamic therapeutic effect for local infections.

Penicillin-G-Acylase (PGA)(EC 3.5.1.11) is a great candidate to be studied using these probes [13,14]. This enzyme could be effectively used for drug delivery purposes, since while it is not naturally produced in eukaryotes, it can operate under in-vivo conditions. Moreover, it is produced in large quantities, which is because of its essential role in production of β-lactam antibiotics such as penicillin and cephalosporin semi-synthetic derivatives. PGA deacylates penicillin G (Pen-G) or cephalosporin G (Ceph-G) to produce the common product phenylacetic acid (PAA), and 6-aminopenicillanic acid (6APA) and 7-amino-3-deacetoxy cephalosporanic acid (7ADCA), respectively. The latter products are the β-lactam nucleus precursors, which undergo further modification during the drug manufacture [15].

Previous studies and models proposed for PGA's reaction with these substrates indicate inhibitory effects, brought by the substrate and the products [16]. There is evidence that suggests the type of inhibition induced by the products could be a function of type of the substrate [17] and even the enzyme's source [18]. Discrepancies between the proposed models do not end at the mechanism level; since the reaction rate constants are affected by pH and temperature. For PGA, it is known that maximum enzyme activity is the in pH range of 7 to 9, and going above 50 °C drastically diminishes enzyme activity [19,20]. In addition to these, other affecting parameters, which are more relevant for industrial purposes, are the immobilization of the enzyme [21] as well as the immobilization methodology [22].

* Corresponding author.
E-mail address: j.h.vanesch@tudelft.nl (JH van Esch).

https://doi.org/10.1016/j.bej.2025.109780
Received 24 February 2025; Received in revised form 30 April 2025; Accepted 9 May 2025
Available online 11 June 2025

Studies on the hydrolysis of Pen-G by PGA, indicate that at high concentrations of Pen-G, the substrate act as an uncompetitive inhibitor. However, this type of inhibition is more evident in enzyme from *Escherichia coli* [16] than from *Bacillus megaterium* [20]. PAA is known to be a competitive inhibitor and 6APA acts as a noncompetitive type of inhibitor [19,23–25]. The applicability of an ordered uni-bi reaction model with substrate inhibition for this system has also been shown [26]. Unlike Pen-G, there are only a few studies on the deacylation of Ceph-G. While Erarslan (1993) identifies PAA as a competitive and 7ADCA as a noncompetitive inhibitor [27], Pan and Syu (2005) reported the opposite for their model, with PAA having noncompetitive inhibition effect and 7ADCA acting as a competitive inhibitor [17]. Although these works point out the substrate's uncompetitive inhibition at high concentrations, the disagreement on products inhibitory effects is striking.

With the exception of the earliest probes based on Fluorescamine [28], which would react with 6APA as the product of hydrolysis leading to indirect detection of PGA, the rest of the developed probes directly exploit PGA's affinity as a hydrolase for breaking linear amides leading to the cleavage of PAA quencher from a fluorophore. Subsequently, these probes are not only highly selective towards PGA but they are also highly sensitive as well, with the ability to detect nanomolar [29] and even sub-nanomolar [13] amounts of PGA. Additionally, they present great capacity for customization, for instance Woronoff et al. (2011) [30] tackled the hydrophobicity of 7-amino-4-methylcoumarin (AMC)-based probe [31] by adding a sulfonate group arriving at a probe with 7-aminocoumarin-4-methanesulfonic acid (ACMS) as the fluorophore, thus fixing the bleeding in their microfluidic apparatus, while keeping the selectivity and sensitivity of the original probe.

A variety of probes are designed for PGA, based on different dye molecules. However, there is a lack of knowledge on the progression of these changes, which is fundamentally important for sensory purposes. Disagreements between models for similar enzyme–substrate systems further necessitate an in-depth study into the kinetics of these probes. Within this study, a suitable model for the kinetics of a fluorogenic probe for PGA is proposed, which is able to simulate the fluorescence retrieval process. The probe is designed inspired by the previous works [3,30] where the fluorescence of an amino-coumarin derivative dye is quenched through formation of an amide bond with phenyl acetate. The unique phenylacetamide-cleaving activity of PGA subsequently causes the removal of the fluorescence emission barrier (PAA) and reinstates the fluorescent signal, Fig. 1. The aforementioned probe can be readily incorporated in a hydrogel, which gained a lot of momentum recently for bio-sensory purposes [32,33], without the disruption of the probe's properties.

2. Methods

2.1. Experimental methods

The probe was prepared according to the description in Supplementary Information (Figure S1 describes the preparation scheme and Figure S2 illustrates QF's ^1H NMR spectrum).

The progress of the reaction was tracked at 25 °C and pH 7.5, using UV–Vis spectrophotometry and spectrofluorometry. The former offers a direct method of measurement, thus it was a fitting candidate for the development of the model. However, the latter is a sensitive method specific to this system, hence it was the chosen methodology to evaluate the kinetic model over lower concentrations.

The low solubility of the probe in buffer was overcome by making a 3 mM stock solution in 10% DMSO. It was further diluted with PBS 1X between 30 to 100 times depending on the concentration targets, which results in 0.3-0.1% DMSO in the medium prior to addition of enzyme, ensuring minimal impact on enzyme activity [34]. At the beginning of each experiment, the cuvette was filled to 690 µL of reactants, the absorption or emission intensity was recorded, then enzyme stock solution was added, leading to a total volume of 700 µL. The enzyme stock solution was prepared by 2000 and 4000 fold dilutions of the enzyme extract with known molar concentration in PBS 1X.

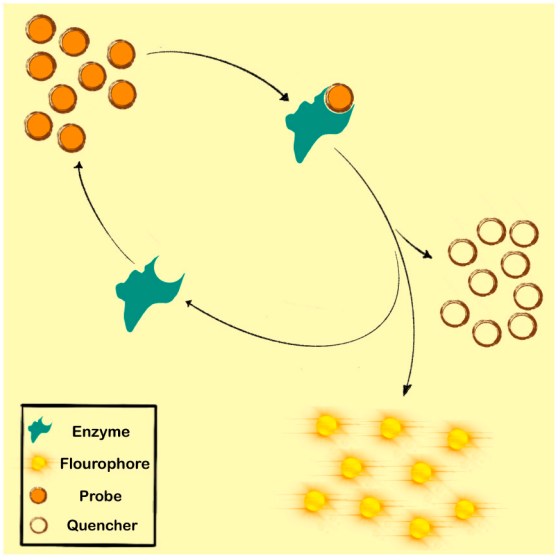

Fig. 1. PGA cleaves off the quencher and reinstates the fluorescence of the probe.

2.1.1. UV-visible spectrophotometry kinetic measurements

The experiments were performed using UV–Vis spectrometer Analytik Jena SPECORD® 250 with attached heat exchanger system (Analytik Jena, Jumo dTRON 08.1) set at 25 °C. Quartz glass cuvettes with 10 mm path length (104-002-10-40, Hellma Analytics) were used with PBS 1X as the reference. The absorption at 341 nm was recorded over time.

2.1.2. Spectrofluorometry kinetic measurements

The experiments were performed using Jasco J-815 CD Spectrometer with fluorescence module. 3-window cells with 20 mm light path length (105-250-15-40, Hellma Analytics) were used. The excitation wavelength was set at 351 nm, and the fluorescence emission spectrum from 300 to 600 nm was recorded, over set time intervals. Then, the intensity progression at 450 nm was tracked.

2.2. Analytical methods

2.2.1. Kinetic model

Fundamentally, the hydrolysis reaction encompasses two substrates: QF and water. The reaction results in formation of two products, both of which show inhibitory effects. The predictions were achieved based on implementation of a simple ordered uni-bi reaction mechanism, where the departure of F from the enzyme's active site occurs prior to the quencher's. Reasoning behind this order, was that Q effectively acts as a competitive inhibitor, which could be viewed as a final step of a sequential bi-product mechanism as well. Additionally, our observations suggest the enzyme-quencher intermediate is not active towards QF.

As shown in Fig. 2, first, the probe forms an intermediate with the enzyme. Next, the fluorophore leaves the intermediate. It reproduces the fluorescent signal and leaves behind the enzyme-quencher intermediate. During the final step, Q leaves the active site of the enzyme. All of the above-mentioned reactions are considered reversible as described in Fig. 2.

2.2.2. Evaluation of the rate constants

For initial velocity analysis, we used the following equation developed for ordered uni-bi reaction mechanism by Cleland [35]:

$$v_{0F} = \frac{\frac{V}{K_{mQF}}\left(C_{QF} - \frac{C_F.C_Q}{K_{eq}}\right)}{1 + \frac{C_{QF}}{K_{mQF}} + \frac{K_{mQ}}{K_{iQ}}\frac{C_F}{K_{mF}} + \frac{C_Q}{K_{iQ}} + \frac{C_F.C_Q}{K_{mF}.K_{iQ}} + \frac{C_{QF}.C_F}{K_{mQF}.K_{iF}}} \quad (1)$$

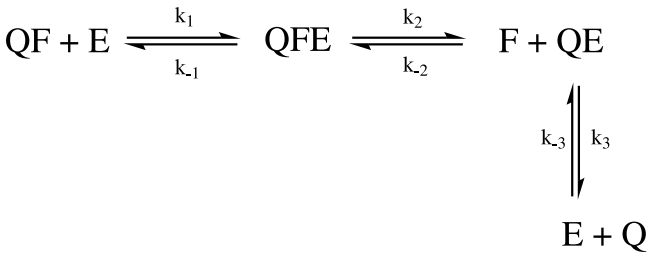

Fig. 2. Ordered uni-bi reaction mechanism for the enzymatic hydrolysis of QF.

Table 1
Michaelis and Inhibition constants.

	Michaelis	Inhibition
Probe	$K_{mQF} = \frac{(k_{-1}+k_2)k_3}{k_1(k_2+k_3)}$	–
Product	$K_{mF} = \frac{k_{-1}+k_2}{k_{-2}}$	$K_{iF} = \frac{k_2+k_3}{k_{-2}}$
Quencher	$K_{mQ} = \frac{k_{-1}}{k_{-3}}$	$K_{iQ} = \frac{k_3}{k_{-3}}$

Where v_{0F} is the initial velocity of product formation($\frac{dC_F}{dt}$). C_{QF}, C_F and C_Q are the initial concentrations of the probe, the product and the quencher, respectively. In the same order, K_{mQF}, K_{mF} and K_{mQ} are the Michaelis constants. K_{iF} and K_{iQ} are inhibition constants for the product and the quencher. Table 1 describes how these constants are defined based on rate constants annotated in Fig. 2.

V is the maximum velocity component as a function of total enzyme concentration (C_E), that is $\frac{k_2 \cdot k_3}{k_2+k_3} C_E$, and the equilibrium constant (K_{eq}) is $\frac{k_1}{k_{-1}} \frac{k_2}{k_{-2}} \frac{k_3}{k_{-3}}$.

In the absence of the product and the quencher($C_F = C_Q = 0$), Eq. (1) changes to simplified Michaelis–Menten formula :

$$v_{0F} = \frac{V \cdot C_{QF}}{K_{mQF} + C_{QF}} \tag{2}$$

Moreover, addition of initial quencher ($C_Q \neq 0, C_F = 0$) causes Eq. (1) to change to:

$$v_{0F} = \frac{V \cdot C_{QF}}{K_{mQF} + C_{QF} + \frac{K_{mQF}}{K_{iQ}} C_Q} \tag{3}$$

Alternatively, addition of initial product in the absence of quencher($C_F \neq 0, C_Q = 0$) leads to:

$$v_{0F} = \frac{V \cdot C_{QF}}{K_{mQF} + C_{QF} + \frac{K_{mQF} \cdot K_{mQ}}{K_{iQ} \cdot K_{mF}} C_F + \frac{1}{K_{iF}} C_{QF} \cdot C_F} \tag{4}$$

For the purpose of computer simulations and parameters estimation, following differential equations were implemented :

$$\frac{dC_{QF}}{dt} = -k_1 \cdot C_{QF} \cdot C_E + k_{-1} \cdot C_{QFE} \tag{5}$$

$$\frac{dC_E}{dt} = -k_1 \cdot C_{QF} \cdot C_E + k_{-1} \cdot C_{QFE} + k_3 \cdot C_{QE} - k_{-3} \cdot C_Q \cdot C_E \tag{6}$$

$$\frac{dC_{QFE}}{dt} = +k_1 \cdot C_{QF} \cdot C_E - k_{-1} \cdot C_{QFE} - k_2 \cdot C_{QFE} + k_{-2} \cdot C_F \cdot C_{QE} \tag{7}$$

$$\frac{dC_{QE}}{dt} = +k_2 \cdot C_{QFE} - k_{-2} \cdot C_F \cdot C_{QE} - k_3 \cdot C_{QE} + k_{-3} \cdot C_Q \cdot C_E \tag{8}$$

$$\frac{dC_F}{dt} = +k_2 \cdot C_{QFE} - k_{-2} \cdot C_F \cdot C_{QE} \tag{9}$$

$$\frac{dC_Q}{dt} = +k_3 \cdot C_{QE} - k_{-3} \cdot C_Q \cdot C_E \tag{10}$$

The numerical solution of the equations, while considering the initial conditions belonging to each experiment, was fitted to the experimental data. LMFIT (Non-Linear Least-Square Minimization and Curve-Fitting for Python) [36] was then employed to numerically solve the system of ODEs, with Levenberg–Marquardt algorithm [37,38], attaining the mixed profiles of F and QF.

2.2.3. Data analysis

Since both the probe and the fluorescent product absorbs at 341 nm, the following equation stands at any point in time:

$$A = A_{QF} + A_F + A_{EC} \tag{11}$$

Where A is the absolute absorption at 341 nm, and A_{QF}, A_F and A_{EC} are the absorption contributions by the probe, the fluorescent product and the enzyme intermediates, respectively. Since the enzyme concentration is much lower than the probe ($A_{EC} \ll A_{QF}$), thus the last term in Eq. (11) is negligible. By omitting the last term and rewriting the equation based on the Lambert–Beer law, Eq. (11) is developed into:

$$A = \epsilon_{QF} \cdot l \cdot C_{QF} + \epsilon_F \cdot l \cdot C_F \tag{12}$$

This equation is used for the simulations, while for initial velocity analysis the first derivative of Eq. (12) is required. Taking the stoichiometry assumption ($-\frac{dC_{QF}}{dt} = \frac{dC_F}{dt}$) into account, the first derivative of absolute absorption is written as:

$$\frac{dA}{dt} = (\epsilon_F - \epsilon_{QF}) \cdot l \cdot \frac{dC_F}{dt} \tag{13}$$

This could also be derived from Eq. (11) with the steady-state assumption $\frac{dA_{EC}}{dt} = 0$.

3. Result and discussion

4-methyl-2-oxo-7-[(phenylacetyl)amino]-2H-chromen-3-yl acetic acid was prepared as the fluorogenic probe for PGA. The acid group could be used for selective connection of the probe onto another entity without the disruption of the fluorogenic property. With the goal of designing a hydrogel sensing device, the acid group offers facile incorporation of the probe on the polymeric chains, for instance via esterification onto polysaccharides. Once prepared, its reaction with the target was studied by analyzing how it progresses over time.

First, the initial velocities were measured for two arrays of similar QF concentrations, implementing UV–Vis spectroscopy, as the first step of analyzing the reaction kinetics. For these experiments, all reaction conditions were kept constant except for the enzyme concentration, which was doubled. The initial velocities were plotted against the initial concentrations of QF over the range 20–50 μM, Fig. 3. These values were attained by linear regression over the reaction progression data between 0–40 s (Figures S3-S8 in Supplementary Information). Subsequently, Eq. (2) was implemented to evaluate V and K_{mQF}. At $K_{mQF} = 73 \pm 29.2$ μM, $V = 0.52 \pm 0.02$ μM/s for the lower enzyme concentration array and it increased to $V = 0.98 \pm 0.26$ μM/s by doubling the enzyme concentration. V appears to be proportional to total enzyme concentration, and such increase is aligned with expectations. Slight discrepancy could be explained by pointing out the error induced by the assumption of initial velocity analysis. In addition to this, no substrate inhibition was observed at this range of substrate concentrations.

Next, complementary analyses at constant enzyme concentration were done to assess the products influence on the kinetics of the reaction. For this purpose, first, initial velocities in presence of varying initial amounts of Q were measured, Fig. 4(a).

The decrease in the initial velocities became apparent by having approximately one order of magnitude larger concentrations of Q in comparison to QF's. Then using the values which were calculated previously, and fitting the data to Eq. (3), K_{iQ} was calculated to be 146.2 ±10.95 μM.

Following that, a similar analysis was performed to determine the influence of F on the reaction kinetics,Fig. 4(b). Although addition of F at the beginning noticeably inhibits the initial product formation velocity, limitations induced by the experimental method complicates accurate characterization. The fact that both QF and F absorb at the chosen wavelength, together with the upper limit on reliable absorbance, impede characterization at the same level of accuracy as the previous step with Q. Consequently, the result of fitting the data to

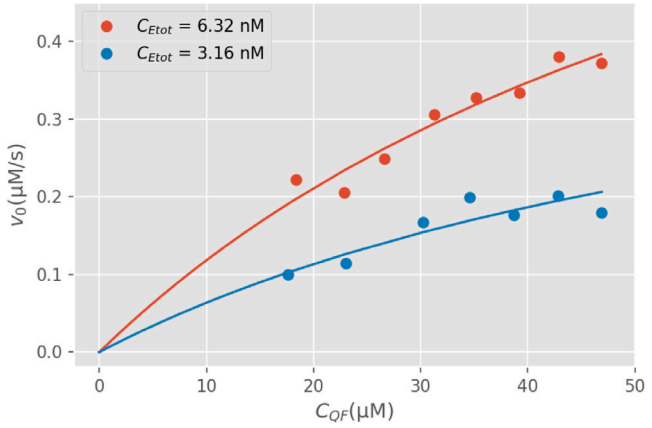

Fig. 3. Initial Velocities as a function of QF concentration. The points represent the experimental data and the line is the fitted curve.

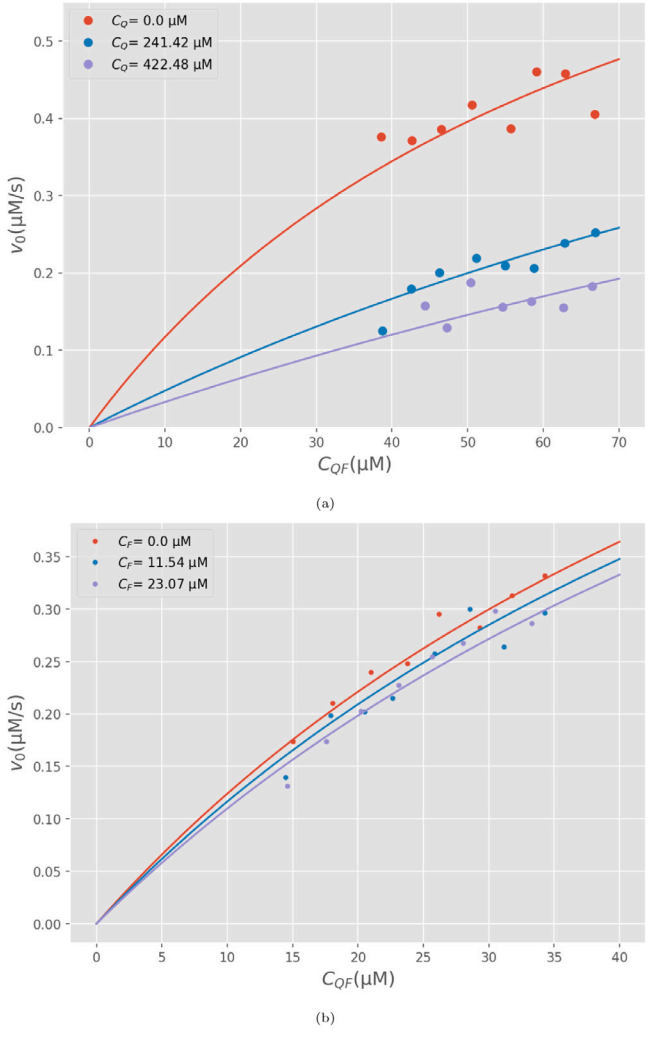

Fig. 4. The influence of addition of products on the initial velocities.

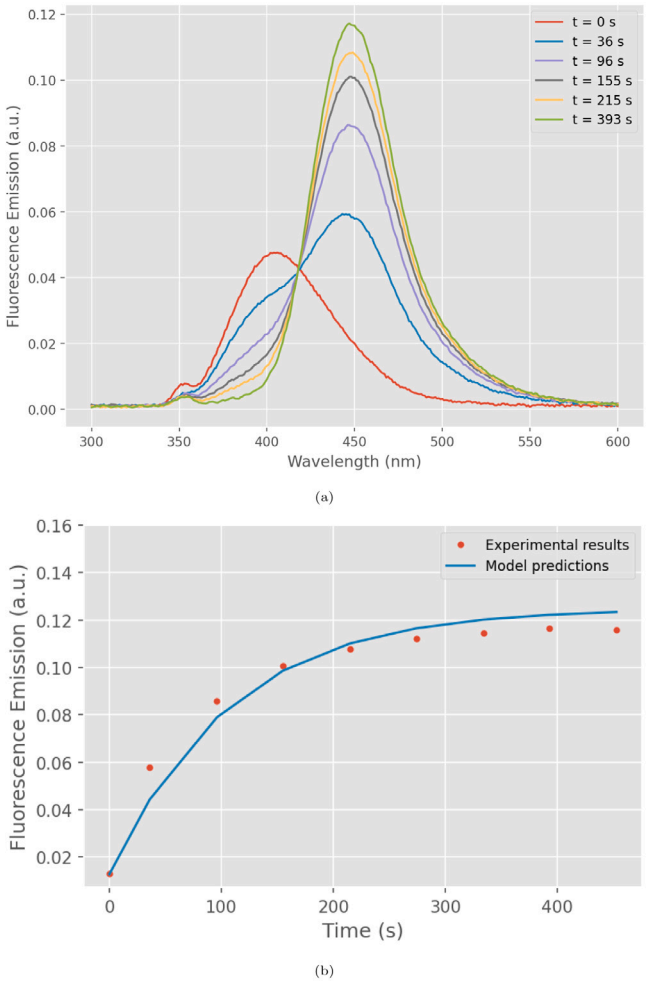

Fig. 5. (a) The progression of the fluorescence emission spectrum for 3.16 nM of PGA and 3.47 μM of QF (b) Progression of the emission intensity at 450 nm.

Eq. (4) comes with an unreliably large margin of error, $K_{iF} = 1.4 \times 10^8 \pm 1.7 \times 10^{13}$.

In order to increase the accuracy, the analytical method was adjusted. Solving the system of ordinary differential equations in Eqs. (5)–(10) and incorporating the resulting concentration profiles into Eq. (12), enables the reconstruction of the absorption signal at 341 nm. By fitting the outcome of the simulation to experimental absorption progress curves, we attempted to estimate the parameters. In order to reduce the bias, the additional control experiments for the initial product's set of experiments were neglected. The rest of the data for the previous analyses were then incorporated at once. The results of the initial velocity analyses was complementary to finding the global optimum.

This approach could effectively reduce the error of the initial velocity measurements, despite being computationally more expensive. The result of fitting over PGA variation, over initial Q variation and over initial F variation are significantly more accurate with average r^2 values of 0.97, 0.99 and 0.94, respectively.

Table 2 shows a summary of the rate constants calculated by initial velocity analysis and corrected with parameter inference. K_{mQF} values are in line with the reports in the literature for similar compounds. However, in case of K_{iF}, there is no comparable value reported for molecules similar to it. At the first glance, K_{iQ} is roughly one order of magnitude smaller than what is reported in the literature. For that work [26], the authors calculated the competitive inhibition constant of Q for the hydrolysis of Pen-G, by enzyme from *Escherichia coli* in

Table 2
Rate constants values; the uncertainty is reported in percentage.

	K_{mQF} (μM)	K_{iF} (μM)	K_{iQ} (μM)
Initial Velocity	73.12 (40%)	1.4×10^8 ($\sim 10^8$%)	146.2 (7.5%)
Parameters Estimation	32.9 (< 1%)	1.2×10^4 (< 1%)	90.9 (< 1%)
Previously Reported	44.7 - 98 [3,30]	–	4.8×10^3 [26]

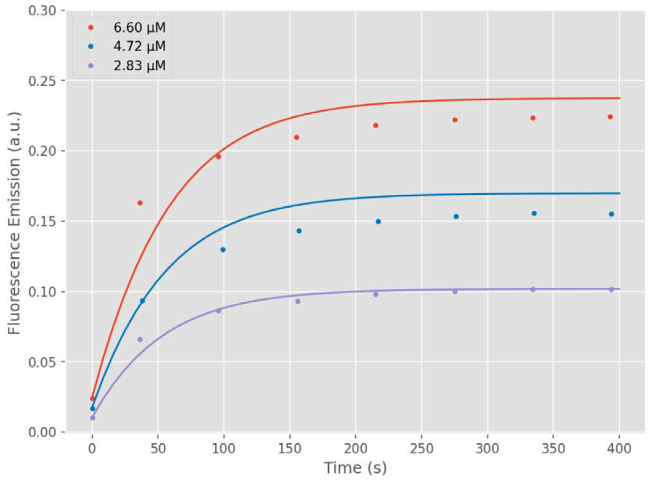

Fig. 6. Experimentally measured change of emission intensity at 450 nm (dots) and model predictions (lines) with 6.32 nM of PGA and 2.83, 4.72 and 6.6 μM of QF.

free state. However, for that study, the pH and the temperature were 8.5 and 37 °C. Higher pH leads to relatively higher amounts of Q in its conjugate base state, which encourages the dissociation of Q from the enzyme. That higher affinity is reflected in the rate constant. In addition to that, although a similar model was implemented, substrate inhibition was also included; which together with K_{iQ} affect the apparent Michaelis constant.

In order to validate the model, its ability to anticipate the fluorescence retrieval process was studied. As shown in Fig. 5(a), over time, the peak belonging to QF at around 400 nm disappears and a new F peak with amplified intensity at 450 nm appears. The final fluorescence emission at 450 nm is almost sixfold larger than the initial emission at that wavelength, with 3.16 nM of PGA and 3.47 μM of QF. The existence of an isosbestic point at around 420 nm further confirms the direct conversion of QF to F, without the formation of side products.

The kinetic model was then employed to reconstruct the fluorescence emission intensity at 450 nm. A similar issue with UV–Vis also persists here that at 450, mixed signals of both QF and F coexist. However, attempting at reconstruction of this signal using modified Eq. (12) is not as direct, since the emission is not linearly proportional to concentration. To tackle this, a linear approximation was done within the concentration range of 1 to 6 μM. This approximation, enabled us to simply test the model in one order of magnitude smaller concentrations of QF, in comparison to the data used for model development, Fig. 5.

Finally the model was further tested with a different concentration of enzyme and varying concentration of QF, Fig. 6 illustrates the results. The slight discrepancy between the model predictions and the experimental results, in particular towards the higher bound of the QF concentrations, could be traced back to deviation in the linear approximation described earlier.

4. Conclusion

A fluorogenic probe for PGA is designed and its fluorogenic property has been shown. Enzymatic hydrolysis of the probe is the driving force behind the retrieval of its fluorescence signal. It was aimed to construct a kinetic model to anticipate the hydrolysis by free PGA. Discrepancies between reported models for similar enzyme–substrate systems called for an investigation into the mechanism. The model was then developed by analyzing the light absorption progression. As expected in the low concentration range of performing the analysis, no substrate inhibition has been observed. However, resulting products were observed to have inhibitory effects on the reaction kinetics. These effects were further characterized and incorporated in an ordered uni-bi type of model structure, via initial velocity analysis and parameter inference. Eventually, the model was validated by simulating the fluorescence emission over the course of the reaction.

CRediT authorship contribution statement

Ardeshir Roshanasan: Writing – review & editing, Writing – original draft, Visualization, Validation, Project administration, Methodology, Investigation, Formal analysis, Data curation, Conceptualization. **Wang Yu:** Investigation, Conceptualization. **Nektarios Katsas:** Investigation. **Jan H. van Esch:** Writing – review & editing, Supervision, Project administration, Investigation, Funding acquisition, Conceptualization.

Declaration of competing interest

The authors declare that they have no known competing financial interests or personal relationships that could have appeared to influence the work reported in this paper.

Acknowledgments

This work is part of a project that received funding from the European Union's Horizon 2020 Research and Innovation Program under the Marie Skłodowska-Curie grant [grant number 812868].

Appendix A. Supplementary data

Supplementary material related to this article can be found online at https://doi.org/10.1016/j.bej.2025.109780.

Data availability

Data will be made available on request.

References

[1] A. Nadler, C. Schultz, The power of fluorogenic probes, Angew. Chem. Int. Ed. 52 (9) (2013) 2408–2410, http://dx.doi.org/10.1002/anie.201209733.
[2] A. Minta, J.P.Y. Kao, R.Y. Tsien, Fluorescent indicators for cytosolic calcium based on rhodamine and fluorescein chromophores, J. Biol. Chem. 264 (14) (1989) 8171–8178, http://dx.doi.org/10.1016/s0021-9258(18)83165-9.
[3] T. Scheper, M. Weiss, K. Schügerl, Two new fluorogenic substrates for the detection of penicillin-g-acylase activity, Anal. Chim. Acta 182 (1986) 203–206, http://dx.doi.org/10.1016/S0003-2670(00)82451-4, URL https://www.sciencedirect.com/science/article/pii/S0003267000824514.
[4] G. Lukinavicius, L. Reymond, E. D'Este, A. Masharina, F. Gottfert, H. Ta, A. Guether, M. Fournier, S. Rizzo, H. Waldmann, C. Blaukopf, C. Sommer, D.W. Gerlich, H.-D. Arndt, S.W. Hell, K. Johnsson, Fluorogenic probes for live-cell imaging of the cytoskeleton, Nature Methods 11 (7) (2014) 731–733, http://dx.doi.org/10.1038/nmeth.2972.

[5] W. Chyan, R.T. Raines, Enzyme-activated fluorogenic probes for live-cell and in vivo imaging, ACS Chem. Biol. 13 (7) (2018) 1810–1823, http://dx.doi.org/10.1021/acschembio.8b00371.
[6] J. Zhang, X. Chai, X.-P. He, H.-J. Kim, J. Yoon, H. Tian, Fluorogenic probes for disease-relevant enzymes, Chem. Soc. Rev. 48 (2) (2019) 683–722, http://dx.doi.org/10.1039/c7cs00907k.
[7] J. Zhang, A. Shibata, M. Ito, S. Shuto, Y. Ito, B. Mannervik, H. Abe, R. Morgenstern, Synthesis and characterization of a series of highly fluorogenic substrates for glutathione transferases, a general strategy, J. Am. Chem. Soc. 133 (35) (2011) 14109–14119, http://dx.doi.org/10.1021/ja205500y.
[8] J. Chin, H.-J. Kim, Near-infrared fluorescent probes for peptidases, Coord. Chem. Rev. 354 (2018) 169–181, http://dx.doi.org/10.1016/j.ccr.2017.07.009.
[9] X. Luo, F. Yu, R. Wang, T. Su, P. Luo, P. Wen, F. Yu, A near-infrared two-photon fluorescent probe for the detection of HClO in inflammatory and tumor-bearing mice, Chin. Chem. Lett. (2024) 110531, http://dx.doi.org/10.1016/j.cclet.2024.110531.
[10] T. Su, R. Shen, D. Tu, X. Han, X. Luo, F. Yu, A β-galactosidase activated near-infrared fluorescent probe for tracking cellular senescence in vitro and in vivo, Smart Mol. 3 (1) (2025) http://dx.doi.org/10.1002/smo.20240062.
[11] C. Zhao, W. Sun, B. Tan, D. Su, Y. Liu, Penicillin G amidase-activatable near-infrared imaging guiding PDT of bacterial infections, Sensors Actuators B: Chem. 382 (2023) 133502, http://dx.doi.org/10.1016/j.snb.2023.133502.
[12] Y. Liu, L. Zhang, K. Liu, L.-L. Wu, H.-Y. Hu, Penicillin G acylase-responsive near-infrared fluorescent probe: Unravelling biofilm regulation and combating bacterial infections, Chin. Chem. Lett. 35 (11) (2024) 109759, http://dx.doi.org/10.1016/j.cclet.2024.109759.
[13] J. Wang, Q. Chen, J. Wu, W. Zhu, Y. Wu, X. Fan, G. Zhang, Y. Li, G. Jiang, A highly selective and light-up red emissive fluorescent probe for imaging of penicillin G amidase inBacillus cereus, New J. Chem. 43 (16) (2019) 6429–6434, http://dx.doi.org/10.1039/c9nj00890j.
[14] L. Li, L. Feng, M. Zhang, et al., Visualization of penicillin G acylase in bacteria and high-throughput screening of natural inhibitors using a ratiometric fluorescent probe, Chem. Commun. 56 (2020) 4640–4643, http://dx.doi.org/10.1039/D0CC00197J.
[15] A. Illanes, P. Valencia, Industrial and therapeutic enzymes, in: Current Developments in Biotechnology and Bioengineering, Elsevier, 2017, pp. 267–305, http://dx.doi.org/10.1016/b978-0-444-63662-1.00013-0.
[16] K. Balasingham, D. Warburton, P. Dunnill, M. Lilly, The isolation and kinetics of penicillin amidase from escherichia coli, Biochim. et Biophys. Acta (BBA) - Enzym. 276 (1) (1972) 250–256, http://dx.doi.org/10.1016/0005-2744(72)90027-7.
[17] J.-L. Pan, M.-J. Syu, Kinetic study on substrate and product inhibitions for the formation of 7-amino-3-deacetoxy cephalosporanic acid from cephalosporin G by immobilized penicillin G acylase, Biochem. Eng. J. 23 (3) (2005) 203–210, http://dx.doi.org/10.1016/j.bej.2005.01.017.
[18] S. Lee, D.D. Ryu, Reaction kinetics and mechanisms of penicillin amidase: A comparative study by computer simulation, Enzym. Microb. Technol. 4 (1) (1982) 35–38, http://dx.doi.org/10.1016/0141-0229(82)90008-4.
[19] A. Erarslan, I. Terzi, A. Güray, E. Bermek, Purification and kinetics of penicillin G acylase from a mutant strain of escherichia coli ATCC 11105, J. Chem. Technol. Biotechnol. 51 (1) (1991) 27–40, http://dx.doi.org/10.1002/jctb.280510103.
[20] C. Chiang, R.E. Bennett, Purification and properties of penicillin amidase from bacillus megaterium, J. Bacteriol. 93 (1) (1967) 302–308, http://dx.doi.org/10.1128/jb.93.1.302-308.1967.
[21] P. Valencia, S. Flores, L. Wilson, A. Illanes, Effect of internal diffusional restrictions on the hydrolysis of penicillin G: Reactor performance and specific productivity of 6-APA with immobilized penicillin acylase, Appl. Biochem. Biotechnol. 165 (2) (2011) 426–441, http://dx.doi.org/10.1007/s12010-011-9262-7.
[22] A.I. Kallenberg, F. van Rantwijk, R.A. Sheldon, Immobilization of penicillin G acylase: The key to optimum performance, Adv. Synth. Catal. 347 (7–8) (2005) 905–926, http://dx.doi.org/10.1002/adsc.200505042.
[23] D. Warburton, K. Balasingham, P. Dunnill, M. Lilly, The preparation and kinetics of immobilised penicillin amidase from Escherichia coli, Biochim. Biophys. Acta - Enzym. 284 (1) (1972) 278–284, http://dx.doi.org/10.1016/0005-2744(72)90066-6.
[24] S.S. Ospina, A. Lopez-Munguia, R.L. Gonzalez, R. Quintero, Characterization and use of a penicillin acylase biocatalyst, J. Chem. Technol. Biotechnol. 53 (2) (1992) 205–213, http://dx.doi.org/10.1002/jctb.280530217.
[25] A. Kheirolomoom, M. Ardjmand, H. Fazelinia, A. Zakeri, Clarification of penicillin G acylase reaction mechanism, Process Biochem. 36 (11) (2001) 1095–1101, http://dx.doi.org/10.1016/s0032-9592(01)00145-5.
[26] D. Warburton, P. Dunnill, M.D. Lilly, Conversion of benzylpenicillin to 6-aminopenicillanic acid in a batch reactor and continuous feed stirred tank reactor using immobilized penicillin amidase, Biotechnol. Bioeng. 15 (1) (1973) 13–25, http://dx.doi.org/10.1002/bit.260150103.
[27] A. Erarslan, The hydrolysis of cephalosporin G by free and immobilized penicillin G acylsse from a mutant of Escherichia coli ATCC 11105, Process Biochem. 28 (5) (1993) 311–318, http://dx.doi.org/10.1016/0032-9592(93)85004-y.
[28] W.L. Baker, Application of the fluorescamine reaction with 6-aminopenicillanic acid to estimation and detection of penicillin acylase activity, Antimicrob. Agents. Chemother. 23 (1) (1983) 26–30, http://dx.doi.org/10.1128/aac.23.1.26.
[29] E.M. Espinoza, J.J. Røise, M. He, I.-C. Li, A.K. Agatep, P. Udenyi, H. Han, N. Jackson, D.L. Kerr, D. Chen, M.R. Stentzel, E. Ruan, L. Riley, N. Murthy, A self-immolative linker that releases thiols detects penicillin amidase and nitroreductase with high sensitivity via absorption spectroscopy, Chem. Commun. 58 (19) (2022) 3166–3169, http://dx.doi.org/10.1039/d1cc05322a.
[30] G. Woronoff, A.E. Harrak, E. Mayot, O. Schicke, O.J. Miller, P. Soumillion, A.D. Griffiths, M. Ryckelynck, New generation of amino coumarin methyl sulfonate-based fluorogenic substrates for amidase assays in droplet-based microfluidic applications, Anal. Chem. 83 (8) (2011) 2852–2857, http://dx.doi.org/10.1021/ac200373n.
[31] M. Ninkovic, D. Riester, F. Wirsching, R. Dietrich, A. Schwienhorst, Fluorogenic assay for penicillin G acylase activity, Anal. Biochem. 292 (2) (2001) 228–233, http://dx.doi.org/10.1006/abio.2001.5078.
[32] A. Herrmann, R. Haag, U. Schedler, Hydrogels and their role in biosensing applications, Adv. Heal. Mater. 10 (11) (2021) 2100062, http://dx.doi.org/10.1002/adhm.202100062.
[33] Z. Tian, L. Feng, L. Li, X. Tian, J. Cui, H. Zhang, C. Wang, H. Huang, B. Zhang, X. Ma, Visualized characterization of bacterial penicillin G acylase for the hydrolysis of β-lactams using an activatable NIR fluorescent probe, Sensors Actuators B: Chem. 310 (2020) 127872, http://dx.doi.org/10.1016/j.snb.2020.127872.
[34] B.-D. Yin, Y.-C. Chen, S.-C. Lin, W.-H. Hsu, Production of D-amino acid precursors with permeabilized recombinant escherichia coli with D-hydantoinase activity, Process Biochem. 35 (9) (2000) 915–921, http://dx.doi.org/10.1016/S0032-9592(99)00157-0.
[35] W. Cleland, The kinetics of enzyme-catalyzed reactions with two or more substrates or products, Biochim. et Biophys. Acta (BBA) - Spec. Sect. Enzym. Subj. 67 (1963) 104–137, http://dx.doi.org/10.1016/0926-6569(63)90211-6.
[36] M. Newville, T. Stensitzki, D.B. Allen, A. Ingargiola, LMFIT: Non-Linear Least-Square Minimization and Curve-Fitting for Python, Zenodo, 2014, http://dx.doi.org/10.5281/ZENODO.11813, URL https://zenodo.org/record/11813.
[37] K. Levenberg, A method for the solution of certain non-linear problems in least squares, Quart. Appl. Math. 2 (2) (1944) 164–168, http://dx.doi.org/10.1090/qam/10666.
[38] D.W. Marquardt, An algorithm for least-squares estimation of nonlinear parameters, J. Soc. Ind. Appl. Math. 11 (2) (1963) 431–441, http://dx.doi.org/10.1137/0111030.